

Review: Probing of the Unoccupied Electronic States in Solids by Inverse Photoemission Spectroscopy

Orhan Zeybek

Balikesir University, Faculty of Science and Arts, Department of Physics, Cagis Campus, Balikesir, Turkey.

ABSTRACT

This paper reviews the probability of probing the unoccupied electronic states in solids by inverse photoemission spectroscopy (IPES). IPES is a surface science technique to analysis the unoccupied electronic states above the Fermi level. IPES is a complementary technique to photoemission. In the IPES technique, the incoming particles are electrons and the outgoing particles are emitted photons that are consequently created by them therefore this technique is named as Bremsstrahlung Isochromate Spectroscopy. This is a common measuring mode because the photons of particular energy are identified. IPES has established one of the most powerful techniques in the study of the unoccupied electronic states in solids.

Keywords:

Inverse photoemission spectroscopy; Photoemission spectroscopy; Unoccupied electronic states; Fermi level; Free–electron–like transitions.

Article History:

Received: 2017/10/07

Accepted: 2017/10/11

Online: 2018/09/30

Correspondence to:

Orhan Zeybek
Balikesir University, Faculty of Science and
Arts, Department of Physics, Cagis Campus,
Balikesir, Turkey

Tel: +90 (537) 524-12 98 /

Fax: +90 (266) 612-12 15

E-Mail: ozeybek@balikesir.edu.tr

INTRODUCTION

In order to probe the electronic structure of a solid, it is useful to know the nature of both the occupied and unoccupied states around the Fermi level (E_F). Inverse photoemission spectroscopy (IPES) is probed the unoccupied electronic states of solids above the E_F [1]. IPES is a complementary surface science technique to the photoemission spectroscopy (PES) which analyses occupied states below the E_F .

In the PES, a photon incident on a sample excites an electron in an occupied state of the sample into an unoccupied state above the E_p , the electron in this final state being the detected particle. In IPES an electron incident on a sample couples into an unoccupied state and makes a radiative transition to another lower lying unoccupied state above the E_p , in this case the emitted photon is detected. The two processes (PES and IPES) for the occupied and unoccupied electronic states are shown in Fig. 1.

In PES a photon promotes an electron in an occupied state below E_F into an unoccupied state above vacuum level (E_{vac}). In IPES an electron that has coupled to an unfilled state above E_{vac} makes a transition into an unoccupied state between E_{vac} and E_F with a emission of photon. In the IPES technique, the incoming particles

are electrons and the outgoing particles are emitted photons, which come from transitions from the free–electron–like incoming electron state into unoccupied states above the E_F of the investigated sample.

More than two decade of work on IPES has considerably advanced the field of study and several reviews at the respective level of maturity were published [2-5]. In early days the development was oriented along known results from PES, which were simply reproduced for the case of unoccupied levels. Problems were tackled which had no precedent in ordinary PES [6]. The unoccupied states can be examined by two-photon photoemission (2PPE) or IPES [2-4]. Because of the low photon energy, 2PPE indicates high energetic resolution.

Theory of Inverse Photoemission Spectroscopy

As it is known in PES process, the sample is bombarded with photons from a UV source. As ultraviolet (UV) photons have lower photon energy than X rays and thus interact only with the electrons in the valence shells or conduction band, the PES can therefore provide information about the electronic band structure of semiconductors and metals. The kinetic energy of the emitted electrons can be calculated by using Equation 1:

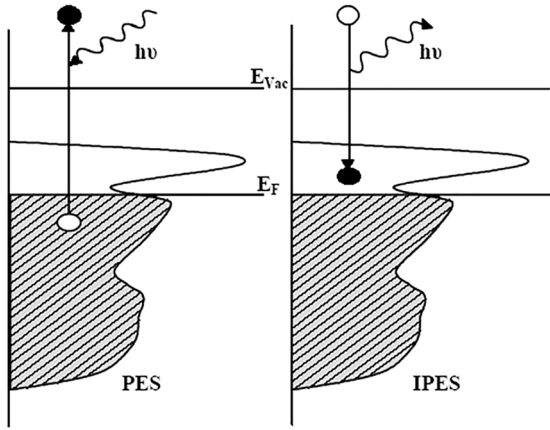


Figure 1. Energy level diagram comparing the PES and IPES processes.

$$KE = h\nu - BE - e\Phi \quad (1)$$

The UV source is a gas discharge lamp. Three source gases were used in these studies, Helium (He), Neon (Ne) and Argon (Ar). The emission lines for He(I) is 21.2 eV, for Ne(I) is 16.8 eV and for Ar(I) is 11.8 eV.

The IPES theory was established by Pendry [7,8]. Pendry exposed that IPES can be defined as PES with the exception of some geometric and phase space coefficients. For the occupied bands [9], k -resolved IPES allows that the energy dispersion $E(k)$ of unoccupied electronic bands can be explained by angle-resolved photoelectron spectroscopy (ARPES).

Pendry [7,8] and Fauster *et al.* [10] declared that the IPES procedure is theoretically the time reversal of PES and two techniques have a Golden Rule, Equation (2) type appearance for the cross section, σ , and the same type of dipole matrix element. Smith *et al.* [11] assumed from molecules that IPES is not the time reversed version of the PES method. IPES contains a transition from the n to $n+1$ electron system. The difference is principally essential near threshold. It should be noted that the primary state in IPES is the final state in PES, and the other way around. As expressed by Himpsel [12], the cross section can be specified as:

$$\sigma \propto (1/j_i) \sum_f |\langle \Psi_f | H_I | \Psi_i \rangle|^2 \quad (2)$$

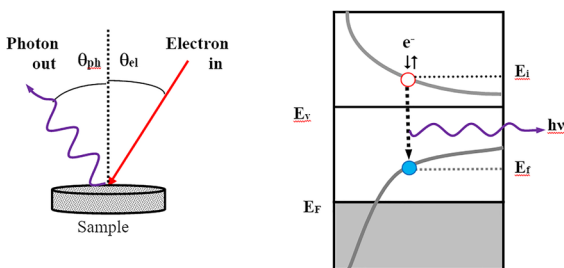


Figure 2. Schematic of the IPES process

where Ψ_i is the initial state with no photons and Ψ_f is the final state contains a band electron plus a photon in IP initial and final states lie above the E_f as shown in Fig. 2. H_I is the interaction Hamiltonian. The dipole matrix element is given by:

$$\langle \Psi_f | H_I | \Psi_i \rangle \propto \int \vec{A} \cdot \vec{J}_f d^3r \quad (3)$$

where \vec{A} is the electromagnetic vector potential. The non-relativistic current takes the form:

$$\vec{J}_f \propto (1/2) e (\Psi_f^* \vec{\nabla} \Psi_i - \Psi_i^* \vec{\nabla} \Psi_f) \quad (4)$$

The experimental development of IPES has been slow compared to PES this is principally as a result of the low cross section for emission of photons in IPES. The ratio of the cross sections [11,13] is specified by:

$$r = \frac{\sigma_{IPES}}{\sigma_{PES}} \approx \left(\frac{\lambda_{el}}{\lambda_{ph}} \right)^2 \equiv \frac{E_{ph}^2}{2m_e c^2 E_{el}} \equiv \alpha^2 \frac{(E_{ph}/R)^2}{4(E_{el}/R)} \quad (5)$$

where λ_{el} and λ_{ph} present the wavelengths of the electron and photon respectively. E_{ph} is the photon energy, E_{el} is the kinetic energy of the electron, m_e is the electron mass, R is the Rydberg constant, and α is the fine structure constant which is $e^2/\hbar c \sim 1/137$. This ratio originates from the different amounts of phase space. The cross section ratio is basically specified by the square of the fine structure constant $\alpha^2 \mu 5 \cdot 10^{-5}$. This constant provides increase to the low quantum yield of IPES ($\sim 10^{-8}$ photons/electron) relative to PES ($\sim 10^{-3}$ electrons/photon, discounting inelastic secondary electrons) [11,13]. Therefore the base signal degrees in IPES are about five times weaker than in PES.

EXPERIMENTAL METHODS IN IPES

IPE experiments can be carried out in two different modes requiring different detection systems. In figure 3, an illustration of the two different IPES modes is shown. Fig. 3(a) represents the isochromat mode, Fig. 3(b) the fluorescence mode. They are developed to make best use of the solid angle of photon collection and the efficiency of photon detection.

Isochromat mode

As shown in Fig. 3(a), the isochromat mode involves scanning the incident electron energy whilst detecting photons emitted at a fixed energy. The isochromat mode is equivalent to the time reversed method of recording ARPES spectra where an electron spectrum is measured for fixed incident photon energy. Detectors for the isochromat mode include the Geiger Muller counter (14). This consists of a stainless steel tube closed at one end by a Calcium Fluoride (CaF_2) entrance window and filled with Iodine gas (I_2). The combination of the transmission

cut-off of the CaF₂ window at high energy and the ionization threshold of the I₂ produce an overall energy window centred around 9.7eV with a bandwidth of 0.8eV. A central electrode floated to a positive potential, collects the electron cascade current generated by any incident photons with an energy lower than the transmission cut-off of the CaF₂ but higher than the ionization potential of the I₂.

Fluorescent mode

As shown in Fig. 3(b), the energy of the electrons in fluorescent mode are hold constant then the energy of the photon is determined with a large aperture grating. This mode allows the initial state constant and obtaining the transitions between the initial and the final state above the E_F. In this circumstance, this mode is easier than in isochromat mode [10].

Momentum (k) Resolved IPES

In an IPE experiment a collimated beam of electrons with a well defined kinetic energy E_{kin} and known incidence angle θ enter a sample. These electrons couple to bulk states of the sample above the E_{vac}. An initial state with energy E_i and wave vector k_i, the electrons possess radioactive decay transitions to the unoccupied final state between E_F and E_{vac} having energy E_f and wave vector k_f. The emitted photons with quantized energy hu are detected at an emission angle α. Applying conservation of energy to the process gives

$$E_i = E_f + h\nu \quad (6)$$

using momentum conservation for the radiative transition yields:

$$k_i = k_f + G + q \quad (7)$$

where G indicates a reciprocal lattice vector and q presents the wave vector of the emitted photon. For low energy photons ~100eV or less the magnitude of q is small compared with the size of the Brillouin zone. It is then a reasonable approximation to neglect G and q in the conservation of momentum, Equation 7 then becomes k_i

= k_f. Initially only the wave vector in the vacuum K of the incident electrons is known. When the electrons enter the sample they experience an attractive force of unknown magnitude due to the crystal potential. The component of the wave vector in the solid k_⊥ is then greater than K_⊥ in the vacuum therefore there is a problem in determining k_⊥ in the final state. The component of the wave vector parallel to the surface is protected because potential is periodic. This results in the condition:

$$k_{\parallel} = k_{i\parallel} + G_{\parallel} \quad (8)$$

where G_∥ indicates surface reciprocal lattice vector. For sufficiently low initial state energies G_∥ = 0 can be used. Then K_∥ is given by:

$$K_{\parallel} = (2m / \hbar^2 (E_f + h\nu - \Phi_s))^{1/2} \sin \theta \quad (9)$$

where φ_s is the workfunction of the sample. It is then possible to determine the final state energy as a function of wave vector parallel to the surface E_f(k_∥) from experimental data, which can be compared with the predicted band structure from theoretical calculations. Experiments are usually done in mirror planes. In mirror planes different bands may become degenerate; this can reduce the complexity of the measured spectra. Also as the wavefunctions of the incoming electrons have even parity they can only couple to initial states of even parity [7], this reduces the number of possible transitions providing a further simplification. The component of the wave vector perpendicular to the surface is not protected. However k may be determined by making an assumption about the initial electronic state. The simplest approximation is of a free electron like initial state with a constant inner potential V₀. At this stage, for normal electron incidence i.e. k_∥ = 0 the wave vector normal to the surface is specified by:

$$k_{\perp} = [2m(E_i - V_0)]^{1/2} / \hbar \quad (10)$$

Other Spectroscopies Used To Study Unoccupied Surface States

A number of other techniques are employed to investigate the unoccupied states above the E_F these include appearance potential spectroscopy (APS) [16], X-Ray absorption spectroscopy (XAS) [17], electron energy loss spectroscopy (EELS) [18], two photon spectroscopy (2PPE) [19], Scanning Tunnelling Spectroscopy (STS) and bremsstrahlung isochromat spectroscopy (BIS). IPES has advantages all above techniques that IPES measures energy E, momentum ħk, spin, energy-band dispersion E(k), and point group symmetry of unoccupied electron state. The uncertainty principle orders that the spatial resolution cannot be of atomic dimensions if the momentum information is to be kept constant [12].

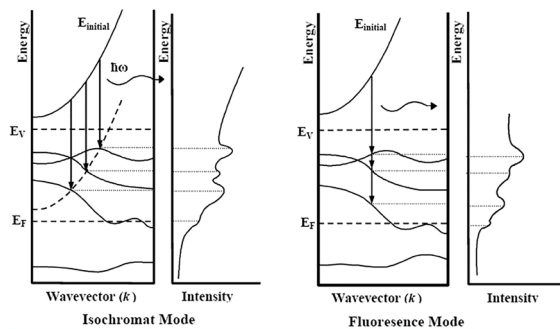


Figure 3. Energy level diagram showing isochromat and fluorescence modes for IPES.

For the XAS, electrons are resonantly excited from an occupied valence-band state to an unoccupied valence-band state. Therefore XAS increases atomic resolution by giving up the momentum information [20] but band mapping as a function of k -parallel is not generally possible.

2PPE determines momentum information, as in IPES. This method is limited to long-lived electronic states [12]. Otherwise, the intermediate state cannot be populated enough without destroying the samples.

STS is a local probe and the problem is the same as XAS. This technique has a very good energy resolution. This method is not limited to vacuum environments but it is less direct than IPES.

In high energy IPE or BIS as it is known, a high energy beam of electrons (~ 1500 eV) is used. For such high energies the momentum of the emitted photon is non negligible and the process is not k -conserving. Therefore BIS reveals little about the wavevector of the unoccupied states, however it is one of the most direct methods for investigating the density of unoccupied states. The use of electrons with energies in the ultraviolet region below ~ 30 eV allows the wave vector and the energy of the unoccupied states above the Fermi level to be probed. For energy of approximately 30 eV the elastic mean free path of electrons is approximately 10 to 20 Å. Therefore low energy IPE is a perfect method for the investigation of the surfaces and interfaces

Experimental Components of IPES

The experimental set up was designed to maximize angle and efficiency of photon because the problems associated with IPES such as: (i) weak signal, (ii) space charge influences that make an upper limit on the incident electron current. Fig. 4 shows the cross section of an advanced IPES spectrometer. It has the following feature: The Spherical Grating (SG), the Multi-Channel Plate (MCP) detector with digital read out and a movable electron gun.

Electron Source of IPES

The electron gun for the IPES experiments was designed to have good energy resolution and was capable of delivering high currents to overcome the low cross section for the production of photons. The thermionic electron emitter was a low work function type BaO source. In this type of electron source, BaO is heated to a temperature high enough (operating at 800 - 1200 °C) to give some electrons sufficient energy to escape the work function barrier at the surface into the vacuum [21,22].

Fig. 5 shows a digital photo of the IPES electron source and analyzer. The electron gun is mounted on a rotatable

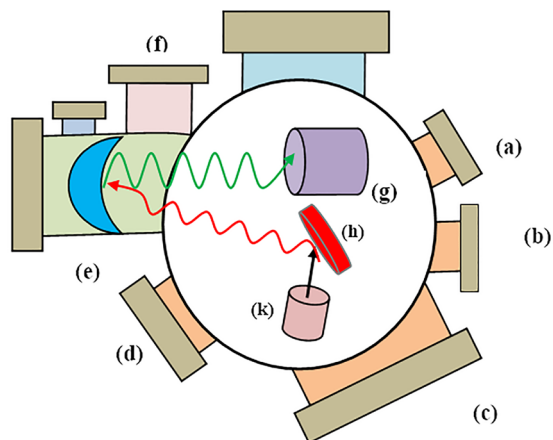


Figure 4. The cross section of the IPES spectrometer (a) X-ray Gun, (b) UV Lamp, (c) Rotatable Electron Gun and Analyser, (d) Window, (e) Spherical Grating, 3600 lines/mm, (f) Shutter and Access, (g) MCP and RAE, (h) Sample, (k) Electron Gun

platform allowing the angle of incidence to be adjusted without disturbing the angle of emission, permitting angle resolved studies. The movable electron gun allows the variation of photon yield with electron direction to be measured at a fixed photon azimuth angle. It is also possible to measure normal and off normal incidence spectra from clean and deposited surfaces with photon emission either near normal or near parallel to the surface which helps distinguish bulk states of different symmetry.

Fig. 6 shows schematic of a Stoffel–Johnson type electron gun [22] which has been used for IPES experiments in this thesis and was designed to give a divergence of $\Delta\theta \sim 5^\circ$ for monoenergetic electrons in the range 5-50 eV.

As shown in figure 6, the electron gun has a circular emitting area of ~ 1 mm diameter, which also determines the diameter of the electron beam. The focal length of the electron gun is electronically adjustable. If the cathode focus distance is risen, the maximum focused current is decreased by radial space charge forces. It was found experimentally that at a typical emission current of 40 μ A and electron energy of 19 eV, then ~ 80 % of the emission current reaches the sample.

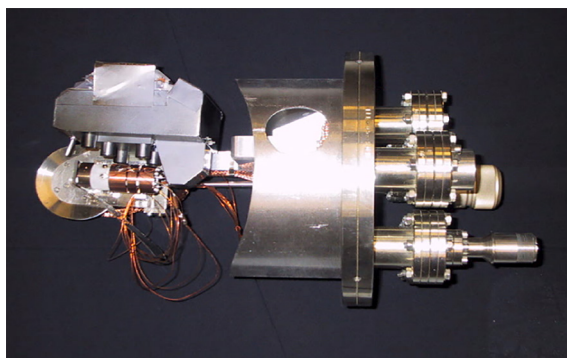


Figure 5. A digital photo of the IPES electron source and analyser

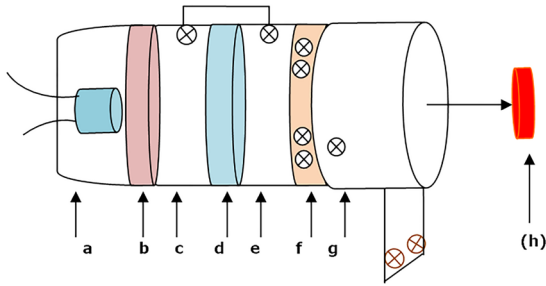


Figure 6. Schematic of the electron optical components of electron gun, (a) BaO cathode, (b) ceramic, (c) anode, (d) ceramic, (e) deflector electrode, (f) ceramic, (g) final lens, (h) sample

Detection system in IPES

The photon emitted from the sample are reflected on Micro-Channels Plates (MCP) detector by a holographic circular diffraction grating which has a diameter of 92 mm, 3600 lines per mm, a concave radius of curvature of 300 mm, and a focal ratio of 3.3. The output of electrons

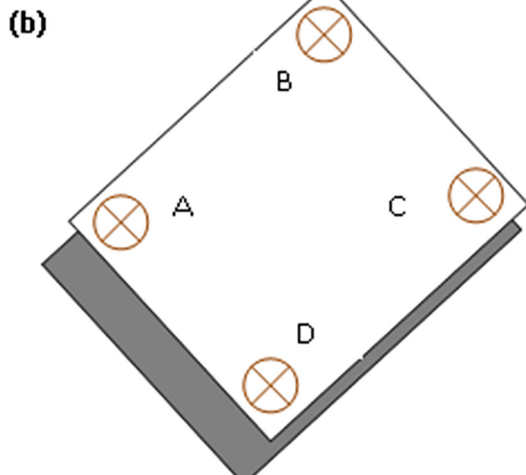
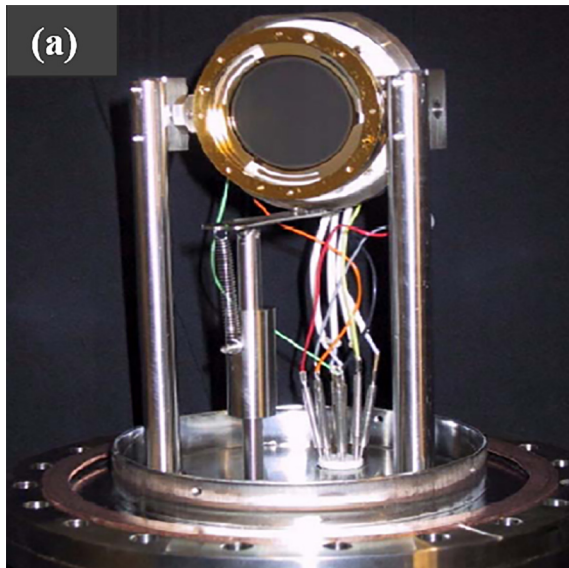


Figure 7. IPES detection system, (a) MCPs, (b) RAE

from the MCP can be seen either straight on a phosphor screen, or indirectly by the charge pulses incident on an anode, as shown in Fig. 7(a), behind the MCPs [23].

The MCP detector assembly, model 3394A supplied by Quantar Technology Inc. USA, has been used. It is made of lead glass with a coating of Nichrome on the surface acting as the electrode. Additionally the front plate is coated in KBr to increase the sensitivity to ultra violet (UV) photons. There are two circular plates of 0.46 mm thickness, back to back with 100 channels along the active diameter of 40 mm. A typical electron gain for the two plate stack is 5×10^6 . It operates in an open face mode with a ratio of $\sim 64\%$. The anodes are shaped resistive sheets.

The photon detection system also includes a position sensitive Resistive Anode Encoder (RAE) behind two MCPs electron multipliers. Each incident electron produces a detectable charge pulse on the resistive anode. The RAE produces charge division between four output electrodes at the corners A, B, C and D, see Fig. 7(b), proportional to the position of the centre of gravity of the charge pulse. The charge sensitive amplifiers convert the low level charge pulses into higher level shaped bipolar pulses suitable for input into the position analyser electronics. The position analyser electronics generates an analogue voltage output proportional to pulse position coordinates that may be calculated from the charges, Q_A, Q_B, Q_C, Q_D collected at the four electrodes:

$$Q_{Tot} = Q_A + Q_B + Q_C + Q_D \quad (11)$$

$$X = \frac{Q_B + Q_C}{Q_{Tot}} \quad (12)$$

$$Y = \frac{Q_A + Q_B}{Q_{Tot}} \quad (13)$$

The AD converters are converted the peak amplitudes from analogue to digital. The coordinates can be calculated using the above formulations. The digital data are moved to a computer for this calculation. The coincidence count rate for the experiments in this thesis is $\sim 200 - 300$ counts per sec. Additional shielding of the resistive anode aperture was provided to make sure that only the reflected photons can reach the detector system.

The setup of the detectors is calculated by the aid of etched polycrystalline copper foil carrying a square grid pattern. An approximate point source ~ 1 mm of electrons is sent on the Cu foil. Photons were emitted toward the mirror and then were reflected onto the MCPs. The four anode channels are established for operation of the peak detection circuits. The images can be figured out by the X and Y coordinates.

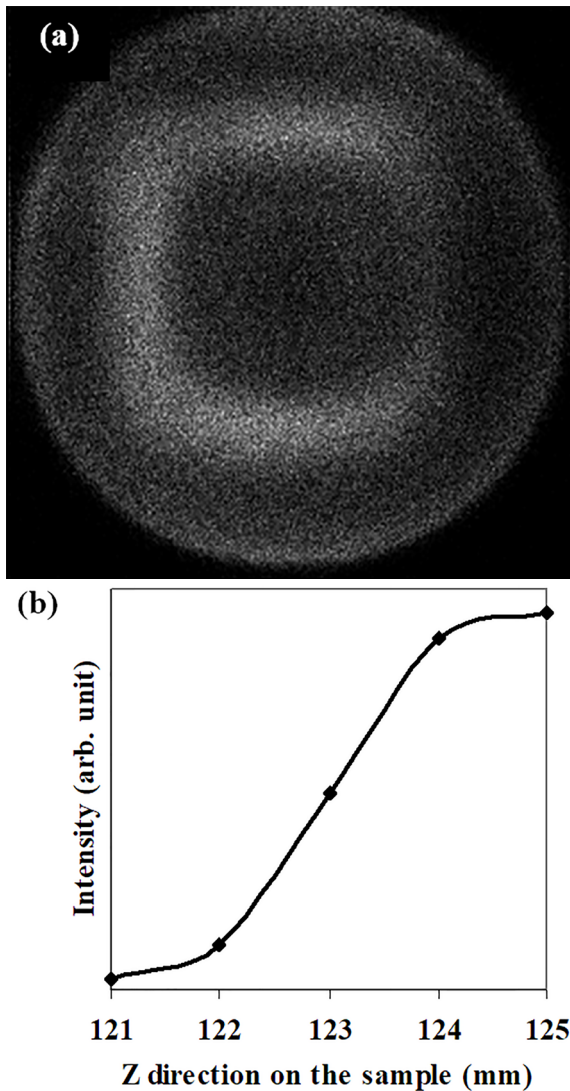


Figure 8. (a) UV illumination Image (b) Intensity vs Cu foil position using IPES.

Fig. 8(a) shows an image of the calibration from the Cu foil, using the latest version of Image SXM software [24]. The calculated $\{X, Y\}$ coordinates are binned into a 256×256 pixels image and expose clearly the over the circular active area of the detector.

In order to get good focusing over the entire area, the detector sample and grating are mounted tangentially to the Rowland circle [25]. This gives a practical linear energy scale over the horizontal coordinate, X direction, of the channel plates. Since the image at the entrance slit does not cover the whole channel plate, it is possible to mask out a narrow band of the slit with aid of the control of the electronics unit.

Energy Resolution of IPES

There are two types of energy resolution, so the first one is the absolute resolution, ΔE , which is described as the Full

Width at Half-Maximum (FWHM) height of a specific measured peak. The second is the relative resolution, R , that is expressed as the ratio of ΔE to the kinetic energy, E_0 of the peak position is given by:

$$R = \Delta E / E_0 \quad (14)$$

For high resolution analysis the measured peak width should be reduced to the lowest possible level. The resolution of the IPES system is controlled by several influences as mentioned below:

1. The thermal energy distribution of the electron beam is one of the influences. The low work function of BaO dispenser cathode used in the electron gun can be operated at temperatures as low as 800 °C. This is found during the degassing of BaO cathode tungsten filament using infrared thermometer. The thermal energy of electrons is given by $3/2(KT)$, where K is the Boltzman constant and T is the cathode temperature in Kelvin. For the cathode temperature of 800 °C, The thermal energy is ~ 0.14 eV.
2. The spot size of the electron beam at the sample is a minimum of ~ 1 mm due to space charge limitation. This is also found experimentally by mounting phosphor screen front of the electron gun.
3. One of procedures of photon collection and photon energy analysis is illustrated schematically in Fig. 9. This method employs a grating spectrograph. The aberration of the grating is the other factor effecting the resolution. Ray- tracing calculations [26,27] for the experimental geometry show that a point source of 19 eV radiation is focused onto the Rowland circle over an area of 90 μm wide and 3 mm high. This represents to an energy resolution of 0.02 eV, which is negligible in comparison to the electron energy spread.
4. The dispersion of the grating can be effected on the total energy resolution of the IPES system but it is negligible in comparison to the electron energy distribution.
5. The spatial resolution of the MCP detector is 0.4 mm. The resolution limit of the grating is small compared to the resolution limit set by the electron beam.
6. The distribution is detected a parabolic dispersion along a particular k-space direction in accordance with:

$$E(k_{\parallel}) = (\hbar^2 / 2m^*)(k_{\parallel} - k_{\parallel}^0)^2 + E_0 \quad (15)$$

where $m^* = (m_{el} \cdot m_{eff})$ and m_{el} is the free electron rest mass, k_{\parallel} is the electron wave vector parallel to the surface, and E_0 provides the bottom of the parabola at k_{\parallel}^0 . According to Equation 15, the momentum resolution of the instrument

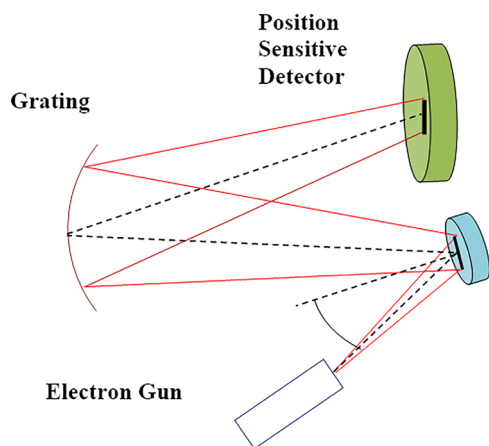


Figure 9. Grating spectrograph with parallel photon detection and analysis in IPES

can be determined by the angular distribution of the incident electron beam at the sample. The electron gun has been designed to produce a full angular distribution of $\Delta\theta \sim 5^\circ$ this gives a momentum resolution of $\Delta k = 0.1 \text{ \AA}^{-1}$ at 5 eV. The momentum broadening is increased to $\sim 0.2 \text{ \AA}^{-1}$ at a beam energy of 20 eV [22]. The total resolution of the IPES system has been determined to be $\sim 0.5 \text{ eV}$ experimentally.

CONCLUSION

One of the main surface science techniques for investigating the empty electronic states is IPES. In this study, IPES is briefly reviewed in the basic physical process for theoretically and experimentally. IPES method can be employed to investigate unoccupied surface states of solids.

ACKNOWLEDGEMENTS

The author acknowledges Balikesir University for the support. The author also sincerely thanks to Dr. S.D. Barrett and A. M. Davarpanah at University of Liverpool Surface Science Research Centre, for their technical assistance.

REFERENCES

- Andrews PT, Collins IR, Inglesfeld JE. Inverse photoemission and how it is used, in: Fuggle JC, Inglesfeld JE (Eds.). Topics in Applied Physics: Unoccupied Electronic States, Fundamentals for XANES, EELS, IPS and BIS. Pp. 243–276, (1992).
- Dose V. Study of empty electronic states by inverse ultraviolet photoemission., *J Phys Chem* 88 (1984) 1681–1690.
- Smith NV. Inverse photoemission. *Rep Prog Phys* 51 (1988) 1227.
- Himpsel F. Inverse photoemission from semiconductors. *Surf Sci Rep* 12 (1990) 3–48.
- Sanada N, Shimomura M, Fukuda Y. Inverse photoemission spectrometer using a BaF₂ window for a low-pass filter. *Rev Sci Instrum* 64 (1993) 3480.
- Yokoyama K, Nishihara K, Mimura K, Hari Y, Taniguchi M, Ueda Y, Fujisawa M. Bandpass photon detector for inverse photoemission spectroscopy. *Rev Sci Instrum* 64 (1993) 87.
- Pendry JB. New Probe for Unoccupied Bands at Surfaces. *Phys Rev Lett* 45 (1980) 1356.
- Pendry JB. A Generalized Friedel Sum–Rule. *Phys C Solid State Physics* 14 (1981) 1137–1143.
- Reihl B, Frank KH. Unoccupied electronic surface states on Cu(110). *Phys Rev B* 31 (1985) 8282.
- Fauster Th, Himpsel FJ, Donelon JJ, Marx A. Spectrometer for momentum-resolved bremsstrahlung spectroscopy. *Rev Sci Instrum* 54 (1983) 68.
- Smith NV, Woodruff DP. Inverse photoemission from metal surfaces. *Prog in Surf Sci* 21 (1986) 295–370.
- Himpsel FJ. Inverse photoemission from semiconductors. *Surf Sci Rep* 12 (1990) 3–48.
- Johnson PD, Davenport JW. Calculated inverse photoemission cross sections from adsorbed molecules. *Phys Rev B* 31 (1985) 7521.
- Smith NV, Chen C, Tranquanda JM, Johnson PD. Unoccupied states on Pd(110) and the surface potential barrier. *Phys Rev B* 38 (1988) 12259.
- Hermanson J. Final-state symmetry and polarization effects in angle-resolved photoemission spectroscopy. *Solid State Commun* 22 (1977) 9–11.
- Park RL, Houston E. L-Shell Soft–X-Ray Appearance–Potential Spectra of the 3d Transition Metals. *Phys Rev B* 6 (1972) 1073.
- Prinz R, Koningsberger K (Eds.). *X-Ray Absorption: Principles, Applications and Techniques of EXAFS, SEXAFS and XANES*, Wiley, New York, 1986.
- Marton L, Lederer LB, Mendlowitz H. Characteristic energy losses of electrons in solids”, *Advances in Electronics and Electron Physics* 7 (1955) 183–238.
- Giesen K, Hage F, Himpsel FJ, Riess JH, Steinmann W. Two-photon photoemission via image-potential states. *Phys Rev Lett* 55 (1985) 300.
- Borca CN, Komesu T, Dowben PA. Comparing inverse photoemission and X-ray absorption spectroscopies. *J Electron Spectrosc Relat Phenom* 122 (2002) 259–273.
- Briggs D, Seah MP (Eds.). *Practical Surface Analysis: Auger and X-Ray Photoelectron Spectroscopy*, second ed. Wiley Interscience New York 1 (1990) 61.
- Stoffel NG, Johnson PD. A low-energy high-brightness electron gun for inverse photoemission. *Nuclear Instruments and Methods in Physics Research A* 234 (1985) 230–234.
- Downie P, Litchfield D, Parsons R, Reynolds DJ, Powis I. High-resolution position-sensing resistive anode microchannel plate detector systems suitable for megahertz count-rates. *Meas Sci Technol* 4: (1993) 1293.
- Barrett SD, Image SXM software. <http://www.liv.ac.uk/~sdb>. Last updated 2017.
- Hutley MC. *Diffraction Gratings (Techniques of Physics)*, Academic Press, 1982.
- Collins IR, Laine AD, Andrews PT, Durham PJ. The unoccupied states of tungsten(001) and tungsten(110): theory and experiment. *J of Physics: Condensed Matter*, 3 (1991) 5307–5321.
- Noda H, Namioka T, Seya M. Geometric theory of the grating. *J Opt Soc Am* 64 (1974) 1031–1036.